# Density-matrix approach for sequential dissociative double ionization of molecules

C. H. Yuen [*] and C. D. Lin[†]

*J. R. Macdonald Laboratory, Department of Physics, Kansas State University, Manhattan, Kansas 66506, USA*

Intense femtosecond infrared (IR) laser pulses have been used in recent years to study the breakup dynamics of molecules. However, observables such as kinetic energy release and branching ratios of molecular fragments are often difficult to predict by theory, making information of the molecular dynamics difficult to retrieve. In this work, we develop a simple model for sequential double ionization of molecules based on a density-matrix approach. The model describes tunneling ionization of the neutral and the ion as well as laser couplings between the ionic states simultaneously. Population of different doubly charged states can be obtained at a low computational cost. We applied our model to $N_2$ and obtained a good agreement on the kinetic energy release spectrum with a previous experiment. This theoretical development could open up the opportunities to use intense short IR laser pulses with coincidence measurement to probe molecular dynamics.

## I. INTRODUCTION

In typical pump-probe experiments, population of the pumped states is much less than the initial state. Ideally, to have good pump-probe signals with high temporal resolution, the probe laser should be intense and as short as a few hundreds of attosecond. Such ultrashort intense light could be generated from x-ray free-electron laser facilities, such as LCLS-II [1] and European XFEL [2], but the beam time is limited. There are also ultrashort laser sources from table-top high harmonic generation [3,4], but the intensity is weak so that the pump-probe signal is weak. In contrast, intense infrared (IR) laser pulses with duration as short as a few femtoseconds are available in most laboratories, and could be useful for probing ultrafast dynamics. However, the probe signal from intense short IR laser pulses is difficult to simulate in general. As a result, it is hard to extract the dynamical information from the measured signal, making such probing schemes unfavorable.

Despite the theoretical challenges, with the emergence of coincidence measurement techniques such as COLTRIMS [5,6] and velocity map imaging [7], there have been increasing interests in strong field double ionization of molecules using intense short IR laser pulses [8–13]. In these experiments, momenta of ionic fragments from different molecular breakup channels and ionized electrons can be measured in coincidence. Observables from the ionic fragments, such as kinetic energy release (KER) spectra and branching ratios, are of particular interests. With certain pump schemes, these measurements could reveal ultrafast molecular dynamics since one expects these observables to be sensitive to the change of ionization energy of some general pumped states. This

strongly motivates the development of theory for strong field double ionization of molecules.

Strong field double ionization can be separated into two regimes: nonsequential and sequential. Nonsequential double ionization dominates when the laser intensity is weak and the second ionization occurs via rescattering of the ionized electron with the residue ion, while sequential double ionization (SDI) dominates when the laser intensity is high and the second ionization proceeds through tunneling ionization of the ion. We are particularly interested in the SDI since one may neglect the impact of rescattering electron and therefore simplify the theory.

There have been some theoretical investigations on the SDI of molecules. One of the modeling studies was done by Tong and Lin [14], who investigated the SDI of $D_2$. Xie *et al.* employed the time-dependent density functional theory to study the SDI of $C_2H_2$ [15]. There are also some recent developments on an *ab inito* approach for SDI by Schlegel and coworkers [16,17]. While the *ab inito* approaches are in general more desirable, they are computationally expensive. To compare with experiments, one often needs to perform angular averaging and volume averaging, which demand a lot of computational time. As a result, such calculations are rarely compared directly to experimental data. Extending these *ab inito* approaches to various pump-probe scenarios appears to be a formidable task. To facilitate the use of intense short IR laser pulses with coincidence measurement for probing molecular dynamics, we develop a simple and efficient model for SDI of molecules, which describes tunneling ionization of the neutral and ionic states and laser couplings between the same charged states simultaneously.

To benchmark our model, we apply it to the SDI of $N_2$ since several aspects of strong field double ionization of $N_2$ have been extensively investigated. On the experimental side, there are studies on charge-symmetric dissociation ($N^+ + N^+$) and charge-asymmetric dissociation ($N^{2+} + N$)

---

[*]iyuen@phys.ksu.edu

[†]cdlin@phys.ksu.edu

[18,19], Coulomb explosion imaging during double ionization [20], and KER and angular distribution of $N^+ + N^+$ [21–23]. There are also spectroscopy studies on $N_2^{2+}$, for example, Auger spectroscopy [24,25] and electron-impact spectroscopy [26], which provide valuable information on the dissociation of different $N_2^{2+}$ states for this work. On the theoretical side, to the best of our knowledge, there has been no investigation on the SDI of $N_2$. But there are some related studies, for instance, lasing of $N_2^+$ by Zhang *et al.* [27], who used a density-matrix approach to describe the population of ionic states and laser couplings between them simultaneously, and the calculation of potential energy curves of $N_2$, $N_2^+$, and $N_2^{2+}$ by Bhattacharya *et al.* [28], which provides additional data for this study.

This article is organized as follows: In the next section, we introduce the density-matrix approach for SDI of molecules and apply it to $N_2$. We then present and discuss our simulated KER spectrum of $N^+ + N^+$ in Sec. III. In Sec. IV, we explore different effects on the KER spectra, such as laser couplings, wavelength dependence, focal volume effect, and alignment effect. Finally, Sec. V summarizes the article and gives outlook for future research.

## II. THEORETICAL APPROACH

After strong field ionization, different charged states of a molecule are still coherent, as long as the laser-molecule system is closed. In the density-matrix formalism, it means that the full density matrix contains nonzero off-diagonal elements between different charged states. However, it is very challenging theoretically to obtain those elements since one would need accurate wave function of the photoelectrons as well as multiple excited states of the ion.

Our goal here is to develop a simple model for SDI of molecules to predict some angle-integrated observables such as KER spectrum and branching ratios. Therefore, at the lowest level of theory, coherence is largely neglected and the full density matrix described here is block diagonal between different charged states. In addition, we neglect the phase differences between the different states of the same charge at the time when they were tunnel ionized. These assumptions are in part consistent with the strong field approximation, which implies that the photoelectron is coupled to the laser field and disentangled with the residue ion, such that the coherence between different states of the same charge and between different charged states are partially lost.

The main approximations of our model can be summarized as follows: (i) Nuclei are fixed during ionization by the laser. (ii) Each charged state is treated as an open system. (iii) Population transfer to higher charged states is treated incoherently and is described by rate equations. (iv) Laser couplings between different states of the same charge are described by the von Neumann equation.

To further simplify the model, in the following, we consider only one neutral state and neglect the laser couplings between the doubly charged states. The nuclear geometry is fixed at the equilibrium of the neutral molecule. Denoting the density matrix of different charged states as $\rho^{(i)}(t)$, where $i = 0, 1, 2$ means the neutral, the ionic, and the doubly charged

states, the time evolutions of density matrices are described as

$$
\begin{aligned}
\frac{d\rho^{(0)}}{dt} &= -\sum_i \rho^{(0)}(t) W_i^{(0)}(t), \\
\frac{d\rho^{(1)}}{dt} &= -\frac{i}{\hbar}[H^{(1)}, \rho^{(1)}] + \Gamma^{(1)}(t), \\
\frac{d\rho_{nn'}^{(2)}}{dt} &= \delta_{nn'} \sum_i \rho_{ii}^{(1)}(t) W_{n \leftarrow i}^{(1)}(t).
\end{aligned}
\tag{1}
$$

The first and the last equation are simply the rate equations for population transfer, where $W_i^{(0)}$ is the ionization rate from the neutral ground state to the $i$th ionic state and $W_{n \leftarrow i}^{(1)}$ is the ionization rate from the $i$th ionic state to the $n$th doubly charged state. The second equation is the von Neumann equation with a source term. The Hamiltonian is $H^{(1)} = H_0^{(1)} + \vec{d} \cdot \vec{E}$, where $H_0^{(1)}$ is the field-free Hamiltonian of the ion, $\vec{d}$ is the dipole moment, and $\vec{E}$ is the laser field. The source term $\Gamma^{(1)}$ describes the population from the neutral state and depopulation to the doubly charged states,

$$
\Gamma_{ij}^{(1)}(t) = \delta_{ij} \left[ \rho^0(t) W_i^{(0)}(t) - \sum_n \rho_{ii}^{(1)}(t) W_{n \leftarrow i}^{(1)}(t) \right].
$$

One can verify that trace of the total density matrix $\sum_i \text{tr}[\rho^{(i)}(t)]$ is conserved by the construction of the equations. Therefore, the population of a state is also the probability of finding the system at that state. Consequently, by setting the initial conditions to be $\rho^{(0)}(t \to -\infty) = 1$ and $\rho^{(1)}(t \to -\infty) = \rho^{(2)}(t \to -\infty) = 0$, probability of forming the $n$th doubly charged state from SDI is $P_n = \rho_{nn}^{(2)}(t \to \infty)$.

As an example, we apply the model to $N_2$ in this article. Our model describes a three-step process for the SDI of $N_2$: (i) HOMO ($3\sigma_g$), HOMO-1 ($1\pi_u$), or HOMO-2 ($2\sigma_u$) of $N_2$ are tunnel ionized to form the $X\ ^2\Sigma_g^+$, $A\ ^2\Pi_u$, or $B\ ^2\Sigma_u^+$ state of $N_2^+$. (ii) The three states of $N_2^+$ are coupled by the laser field while being further tunnel ionized to form different doubly charged states. (iii) The doubly charged states may then dissociate to their respective limits.

The relevant potential energy curves for $N_2$, $N_2^+$, and $N_2^{2+}$ states from Ref. [28] are shown in Fig. 1. For brevity in this article, $X$, $A$, and $B$ states always refer to the $X\ ^2\Sigma_g^+$, $A\ ^2\Pi_u$, and $B\ ^2\Sigma_u^+$ state of $N_2^+$, while states 1–11 always refer to the $N_2^{2+}$ states in Table I. The equilibrium position of $N_2$ at $R = 1.09\ \text{Å}$ is marked by the vertical line in Fig. 1. The $X$ and $A$ states and the $X$ and $B$ states are coupled by a dipole moment of $d_x = 0.25a_0$ [29] and $d_z = 0.75a_0$ [30]. Doubly charged states that dissociate are labeled as states 5–11 in Fig. 1, and the details about states 1–11 of $N_2^{2+}$ can be found in Table I. Note that states 1–4, which have a hole in the HOMO, are not shown in Fig. 1 as they are metastable. In other words, all $N_2^{2+}$ states that contribute to the KER spectrum come from ionization of the excited states of $N_2^+$.

The key elements in our model are the ionization rates. In our current approach, we used the MO-ADK formula [31] for the ionization rates $W^{(0)}$ from $N_2$ to $N_2^+$ and $W^{(1)}$ from $N_2^+$ to $N_2^{2+}$. For the first ionization, the structural parameter of $N_2$ from Zhao *et al.* [32] and experimental ionization energy of 15.58, 16.93, and 18.75 eV for HOMO, HOMO-1, and
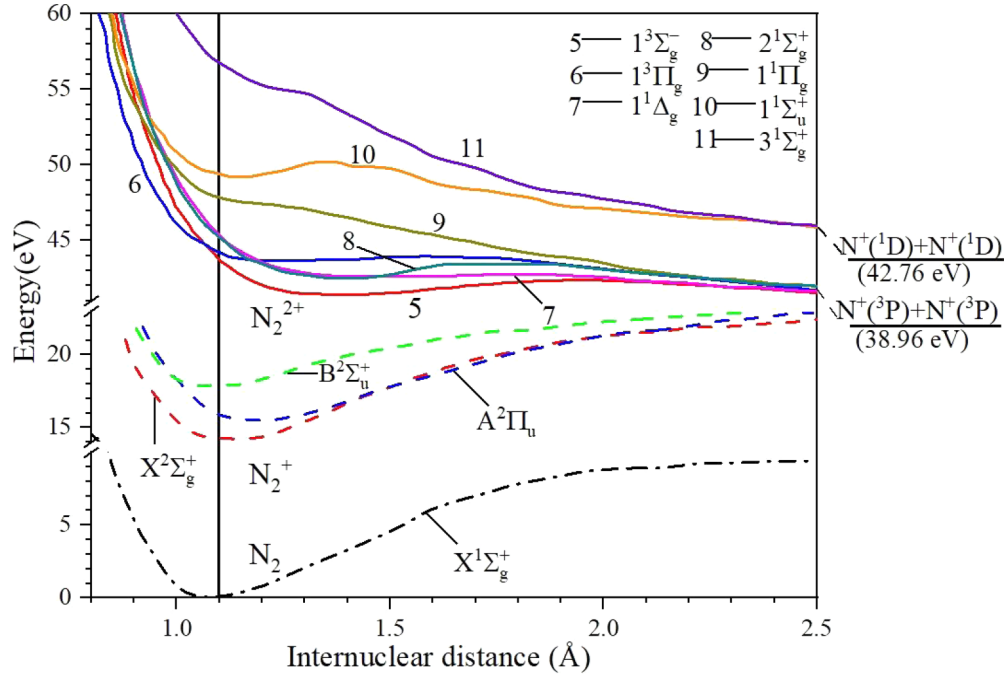
FIG. 1. Potential energy curves for $N_2$, $N_2^+$, and $N_2^{2+}$, adopted from Ref. [28]. The first four states of $N_2^{2+}$ are metastable and are omitted in the figure to avoid overcrowding.

HOMO-2 were used. For the second ionization, we assume the structural factor of the HOMO, HOMO-1, and HOMO-2 of $N_2^+$ are the same as of $N_2$ but the ionization energies are different. The ionization energy used in $W_{n \leftarrow i}^{(1)}$ is obtained by subtracting vertical ionization energy of the $n$th state in Table I by the ionization energy to the $i$th $N_2^+$ state. Meanwhile, the structural factor used in $W_{n \leftarrow i}^{(1)}$ is determined by which orbital of $N_2^+$ to be removed to reach to the $n$th state. For example, state 6 has holes in the HOMO-1 and HOMO-2, and can be reached either from the $A$ state by removing an electron in HOMO-2 or from the $B$ state by removing an electron in HOMO-1. The ionization energy to state 6 from the $A$ and

from the $B$ state are then 29.49 and 27.67 eV, respectively. With the ionization rates and initial conditions, Eqs. (1) are then solved numerically by the classic Runge-Kutta method.

Throughout this article, the laser pulse takes the form of

$$\vec{E}(t) = E_0 e^{-2\ln 2(t^2/\Gamma^2)} \cos \omega t \, \hat{\epsilon},$$

where $\Gamma$ is the full width at half-maximum (FWHM), $\omega$ is the central frequency, and $\hat{\epsilon}$ is a polarization vector on the $xz$ plane. We chose the molecular axis of $N_2$ to be fixed on the $z$ axis and the laser to propagate along the $y$ axis. FWHM of the pulse is fixed at 8 fs throughout this article since a longer pulse

TABLE I. Vertical ionization energy to the $N_2^{2+}$ states with two valence holes. Ionization energy ($I_p$) to $N_2^{2+}$ are taken from Bhattacharya *et al.* [28]. Dissociation limits of the $N_2^{2+}$ states are taken from Iwayama *et al.* [25]. The limit of the $1\,^1\Sigma_u^+$ and $3\,^1\Sigma_g^+$ states are identified from the PEC from Ref. [28]. Metastable states are marked as m.s. in the table.

| Index | $N_2\,(...2\sigma_u^2 1\pi_u^4 3\sigma_g^2)\,^1\Sigma_g^+$ States | Config. | $I_p$ (eV) | Limit | KER (eV) |
|---|---|---|---|---|---|
| 1 | $1\,^1\Sigma_g^+$ | $3\sigma_g^{-2}$ | 42.7 | m.s. | |
| 2 | $1\,^3\Pi_u$ | $1\pi_u^{-1} 3\sigma_g^{-1}$ | 43.59 | m.s. | |
| 3 | $1\,^3\Sigma_u^+$ | $2\sigma_u^{-1} 3\sigma_g^{-1}$ | 44.11 | m.s. | |
| 4 | $1\,^1\Pi_u$ | $1\pi_u^{-1} 3\sigma_g^{-1}$ | 45.12 | m.s. | |
| 5 | $1\,^3\Sigma_g^-$ | $1\pi_u^{-2}$ | 45.69 | $N^+(^3P) + N^+(^3P)$ | 6.73 |
| 6 | $1\,^3\Pi_g$ | $2\sigma_u^{-1} 1\pi_u^{-1}$ | 46.42 | $N^+(^3P) + N^+(^3P)$ | 7.46 |
| 7 | $1\,^1\Delta_g$ | $1\pi_u^{-2}$ | 46.72 | $N^+(^3P) + N^+(^3P)$ | 7.76 |
| 8 | $2\,^1\Sigma_g^+$ | $1\pi_u^{-2}$ | 46.72 | $N^+(^3P) + N^+(^3P)$ | 7.76 |
| 9 | $1\,^1\Pi_g$ | $2\sigma_u^{-1} 1\pi_u^{-1}$ | 49.12 | $N^+(^3P) + N^+(^3P)$ | 10.16 |
| 10 | $1\,^1\Sigma_u^+$ | $2\sigma_u^{-1} 3\sigma_g^{-1}$ | 50.57 | m.s./$N^+(^1D) + N^+(^1D)$ | 7.81 |
| 11 | $3\,^1\Sigma_g^+$ | $2\sigma_u^{-2}$ | 57.4 | $N^+(^1D) + N^+(^1D)$ | 14.64 |

would allow the nuclei to move appreciably during ionization. We also chose $t = 0$ to be at the peak of the pulse envelope.

As a side note, we want to emphasize that our model also provides a general framework to extend to different scenarios. For example, the ionization rate $W^{(1)}$ in Eqs. (1) could be replaced by excitation or ionization rates by rescattering electron, such that nonsequential double ionization can be modeled. One can also include higher charged states in Eqs. (1) to model multiple ionization and Coulomb explosion. There is room for improvement in the model for SDI as well. For instance, it is possible to model the coherence in SDI by following the approach by Xue *et al.* [33] for $O_2^+$. It is also possible to model SDI coherently and more accurately in this framework if accurate single ionization rates are available from some quantum chemistry methods.

## III. MAIN RESULTS

The observable we are interested for SDI of $N_2$ is the KER spectrum of the $N^+ + N^+$ channel. We aim to reproduce the experimental result by Voss *et al.* [21], who used a laser with peak intensity $1.2 \times 10^{15}$ W/cm², 8 fs FWHM, and 800 nm wavelength. By solving Eqs. (1), we obtain the probability of forming different $N_2^{2+}$ states at different angles $\theta$ between the laser polarization and the molecular axis. Assuming the molecule is randomly oriented, the angular-averaged probabilities for the $n$th $N_2^{2+}$ state are obtained by

$$\bar{P}_n = \frac{1}{2} \int_0^{\pi} P_n(\theta) \sin \theta \, d\theta. \tag{2}$$

Since the KER of different $N_2^{2+}$ states are known from Table I, the intensity of the KER spectrum is simply given by their angular-averaged yield. To compare with the experiment by Voss *et al.* [21], the probabilities are convoluted with a Gaussian distribution,

$$S(E) = \sum_n \frac{\bar{P}_n}{\sqrt{2\pi\sigma^2}} \exp\left[-\frac{(E - E_n)^2}{2\sigma^2}\right], \tag{3}$$

where $E_n$ is the KER of state $n$ and $\sigma$ is set to 0.28 eV since the energy resolution for KER in the experiment was less than 0.3 eV.

The top panel of Fig. 2 shows the simulated KER spectrum and the experimental data by Voss *et al.* [21]. Overall, position of peaks and ratios between peak values from our simulated KER spectrum agrees excellently with the experiment. The ratio between the first to the second peak and the third to the second peak from our results are about 0.52 and 0.09, while in the experiment by Voss *et al.* [21], those ratios are roughly about 0.54 and 0.12. We note that the KER spectra from Wu *et al.* [19,23] are similar to ours and to Voss *et al.* [21], even though the laser parameters they used were different.

Despite the good agreement between our results and the experiment, the experimental spectrum is considerably broader. The onset of the first peak in the experiment is at about 5 eV, but it is at about 6 eV in our case. In the experiment, the third peak overlaps with the second peak, but in our case they are well separated. These seem to suggest that each peak is broadened by about 1 eV in the experiment. One possible cause for the broadening is the vibrational motion of $N_2$ since
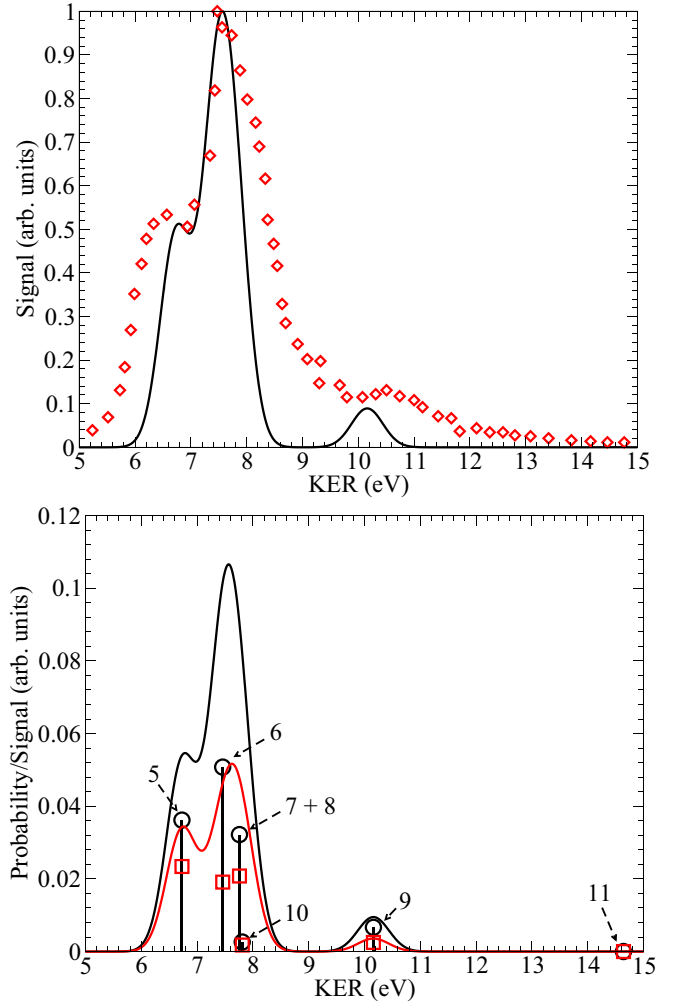


FIG. 2. Top: Comparison between our simulated KER spectrum (solid line) and the experimental data by Voss *et al.* [21] (symbols). Both spectra are normalized to their highest peak. Bottom: Angular-averaged yield for dissociative $N_2^{2+}$ states, obtained with (circle) and without (square) the laser couplings between different $N_2^+$ states. Black and red solid lines are the results convoluted with a Gaussian distribution. The laser used is linear polarized with peak intensity $1.2 \times 10^{15}$ W/cm², 8 fs FWHM, and 800 nm wavelength.

KER of different $N_2^{2+}$ states could change significantly in the Frank-Condon region. For example, from Fig. 1, ionization energies of state 5 at $R = 1.0$ and 1.2 Å are about 47 and 42 eV, giving KER of about 8 and 3 eV, respectively. If one can improve the energy resolution of the detector as in Ref. [26], contribution from different vibrational states could then be identified, and one can verify whether the broadening is due to the vibrational motion. If the broadening is indeed resulted from the vibrational motion, then branching ratios of fragmentation channels could be insensitive to such motion since the ratios are obtained by integrating the signal along the KER axis. Consequently, a fixed-nuclei model could be sufficient if one is interested only in branching ratios. While one can take the vibrational motion into account by calculating the angular-averaged yield at different $R$ and averaging it with a

nuclear wave function or by the approach in Ref. [14], it is beyond the scope of this study.

Although we have calculated the yield of different $N_2^{2+}$ states at different angles, we are not intended to compare the angular distribution with experiments. The main reason is that at high laser intensity, one should include the post-ionization alignment of the ionic fragments [34] and propagate the nuclear wave packet in the field-free Hamiltonian for each fragmentation channel since the angular distribution from the model could be significantly modified.

## IV. EFFECTS ON KER SPECTRA

With the low computational cost, we can explore different effects on the KER spectrum from SDI efficiently. In the following, we look into the effect of laser couplings, wavelength dependence, effect of focal volume, and the alignment dependence. Pathways leading to different KER peaks can be deduced from studying some of these effects.

### A. Laser couplings

To investigate the effect of laser couplings on the KER spectrum, we solve Eqs. (1) without the commutator term for the ionic states. This turns Eqs. (1) to simply a set of rate equations. Circle and square symbols in the bottom panel of Fig. 2 show the angular-averaged yield of dissociative $N_2^{2+}$ states with and without the laser couplings. For both cases, angular-averaged yield of dissociative $N_2^{2+}$ states are in the order of $10^{-2}$, although population of the neutral and ionic states are depleted by the end of the pulse. This is because most of the population are in states 1–4 (see Fig. 5 for details). We found that the first KER peak at 6.77 eV mostly comes from state 5, the second peak at 7.58 eV comes from the overlap of states 6–8, and the third peak at 10.16 eV comes from state 9. States 10 and 11, due to their relatively large ionization energies, have negligible population compared to the other states. The major differences between the two cases are the decrease of yield when the laser couplings are neglected. For example, without the couplings, yield of state 6 drops about 62%, while yield of states 5, 7, and 8 drop about 35%. To see the impact on the KER spectrum, the results with and without the couplings are convoluted and shown as black and red solid lines in the lower panel of Fig. 2. We see that in the case without the couplings, the second peak shifts slightly to the right, and the peak value is about a factor of 2 smaller compared to the case with the laser couplings. The ratio between the first to second peak and the third to second peak are 0.66 and 0.07 without the couplings, which are about 30% larger and 20% smaller than the case with the couplings. Although the ratio between the peaks does not change significantly, the overall decrease of angular-averaged yield suggests that laser couplings play an important role in SDI.

To further understand the role of laser couplings, we look into the populations of different $N_2^+$ states with and without the laser couplings when polarization of the laser is 45° from the molecular axis. This angle is chosen since both the $X$ and $A$ states and the $X$ and $B$ states would be coupled by the laser. Top and bottom panels in Fig. 3 show the population of the three $N_2^+$ states as a function of time without and with the laser
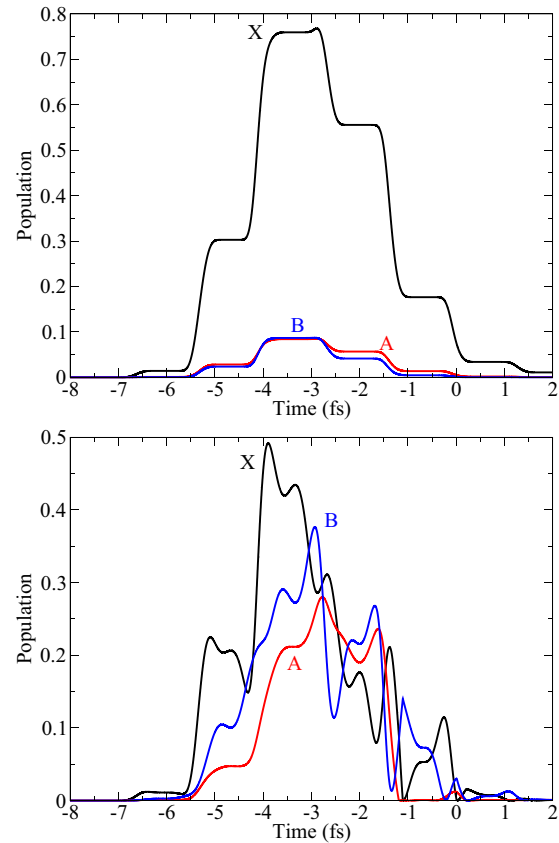


FIG. 3. Population of the $X\ ^2\Sigma_g^+$ (black), $A\ ^2\Pi_u$ (red), and $B\ ^2\Sigma_u^+$ (blue) states of $N_2^+$ as a function of time. The bottom and the top panels are the results with and without the laser couplings. The laser polarization is 45° from the molecular axis. Other laser parameters are the same as in Fig. 2.

couplings. The other laser parameters are the same as in Fig. 2. Without the laser couplings, the populations of states are simple step functions corresponding to the population from the neutral state and the depopulation to the doubly charged states. Shortly after $t = -4$ fs, where the instantaneous laser intensity is half of the peak, the neutral population is depleted. The ionic population is at the maximum and is dominated by the $X$ state with peak value at about 0.75, while the $A$ and $B$ states both have populations slightly less than 0.1. The ionic population then drops rapidly with increasing instantaneous laser intensity. As the laser reaches to the peak value at $t = 0$ fs, most of the ions have been tunnel ionized to $N_2^{2+}$. For the case with the laser coupling, populations of the ionic states have significant modulation on top of the population and depopulation process. The maximum population of the $X$ state is about 50% smaller, while the maximum populations of $A$ and $B$ states are about three times larger than the case without the couplings. Surprisingly, population of the $B$ state shows a stronger enhancement than the $A$ state, even though the energy difference between the $X$ and $A$ states (1.35 eV) is closer to the photon energy (1.55 eV).

Comparing the $N_2^+$ population with and without laser couplings, we see that laser couplings strongly enhance the population of ionic excited states, which eventually leads to higher probabilities for forming dissociative $N_2^{2+}$ states. In
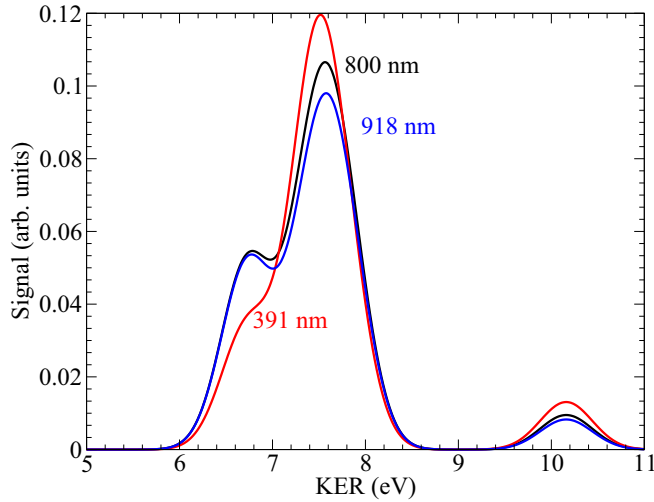
FIG. 4. KER spectra as in Fig. 2 for a 800-nm (black), 391-nm (red), and 918-nm (blue) laser.



FIG. 5. Intensity dependence of the angular-averaged yield for different $N_2^{2+}$ states.

addition, from Fig. 3, one can further deduce that the KER spectrum will not be sensitive to the carrier-envelope phase of the laser, as most of the ions would have been ionized at some other time. The same argument applies to the dependence on the pulse duration, as long as the pulse is short enough such that the nuclei can be regarded as fixed during ionization. Our calculations confirmed that these are indeed the cases, where the ratio between the first to second peak in the spectrum changes by at most 2% and 1% for different pulse durations (5–8 fs) and carrier-envelope phases ($0$–$\pi$), respectively.

### B. Wavelength dependence

Since the inclusion of laser couplings is important, it implies that the KER spectrum could be significantly different if the photon energy matches the excitation energy of the ion. Therefore, we calculate the KER spectra for a 391- and 918-nm laser, which have photon energy of about 3.17 and 1.35 eV, to match the excitation energy between the $X$ to $B$ state and the $X$ to $A$ state. Other laser parameters are the same as in Fig. 2.

The wavelength dependence provides a good example to illustrate the formation mechanism of different states of $N_2^{2+}$. For examples, state 6 can be formed from the $A$ or $B$ state, but states 5, 7, and 8 can only be formed from the $A$ state. If the population of the $A$ state during ionization is suppressed, population of states 5, 7, and 8 are also suppressed. However, the same may not be true if the $B$ state is suppressed, as the ionization yield to state 6 from the $A$ state or the $B$ state obtained by the MO-ADK theory are about the same. Therefore, even if the $B$ state is suppressed during ionization, population of state 6 may not change much.

Figure 4 shows the KER spectra obtained with a 800-, 391-, and 918-nm laser. The spectrum from the 918-nm laser is quite similar to the 800-nm one, where the main peak at 7.6 eV is only about 7% smaller than the 800-nm result. This is because state 6 is slightly less populated due to less $B$ state during ionization, while the populations of states 5, 7, and 8 are about the same as the 800-nm result. On the other hand, the spectrum
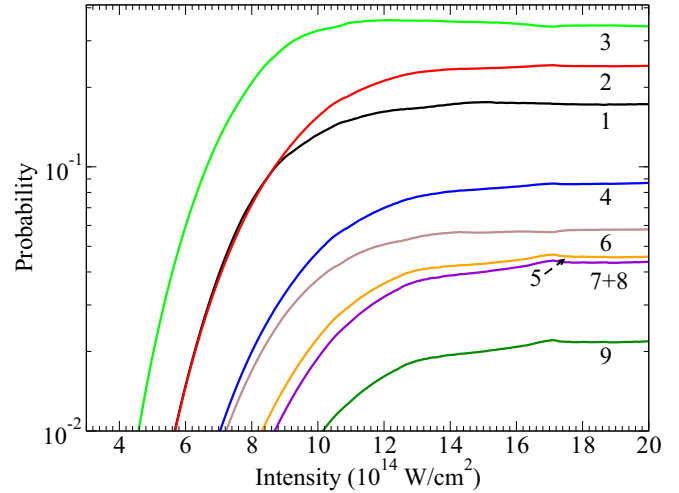
from the 391-nm laser shows a stronger suppression on the first peak at 6.8 eV and a 13% enhancement on the second peak. The suppression of the first peak is a consequence of having less $A$ state being populated during ionization, while the enhancement of the second peak comes from the increase of population of state 6, which comes from the increase of population of the $B$ state during ionization. Our results show that it is possible to weakly control the KER spectrum from SDI and identify the key intermediate states in the SDI process by changing the wavelength of the laser. Wavelength dependence on nonsequential double ionization of $O_2$ was studied by Alnaser *et al.* [35] and they found significant dependence in the KER spectra of $O^+ + O^+$ using 50-fs lasers. The weak dependence in our case could be due to the fact that we use 8-fs short pulses which have a broader bandwidth, therefore, the KER spectra are less sensitive to resonance conditions.

### C. Intensity dependence

When the laser is focused tightly, the laser intensity inside the focal region is not constant, SDI at different intensities within the focal volume should be considered in order to compare with experiments. It is therefore of interest to investigate the intensity dependence of the dissociative SDI yield and access the importance of focal volume averaging. Laser parameters used in this section are the same as in Fig. 2, except the laser intensity.

Figure 5 shows the angular-averaged yield for states 1–9 at different peak laser intensities. One can see that states 1–3 are the dominant channels as their ionization energies are the lowest. When the intensity is about $7 \times 10^{14}$ W/cm$^2$, the yield of state 6 reaches to about $10^{-2}$. As the intensity is about $1.2 \times 10^{15}$ W/cm$^2$, SDI to states 1–9 starts to be saturated. As a result, when the peak intensity at the focus is $1.2 \times 10^{15}$ W/cm$^2$, gases away from the focus will also be ionized to form states 5–9.

The spatial profile of a tightly focused laser can be modeled as a Gaussian beam. Assuming the gas volume is larger than the laser focus volume, the volume-averaged probability for
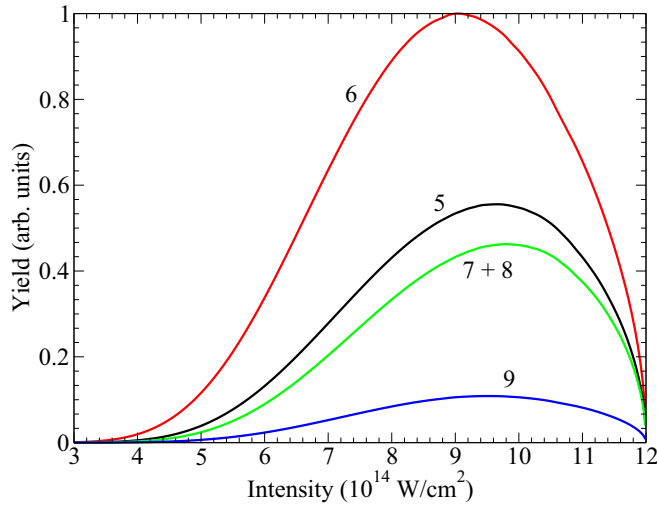
FIG. 6. Differential intensity dependence with peak intensity $1.2 \times 10^{15}$ W/cm$^2$ on angular-averaged yield of states 5–9. The yield is normalized to the peak of the curve of state 6.
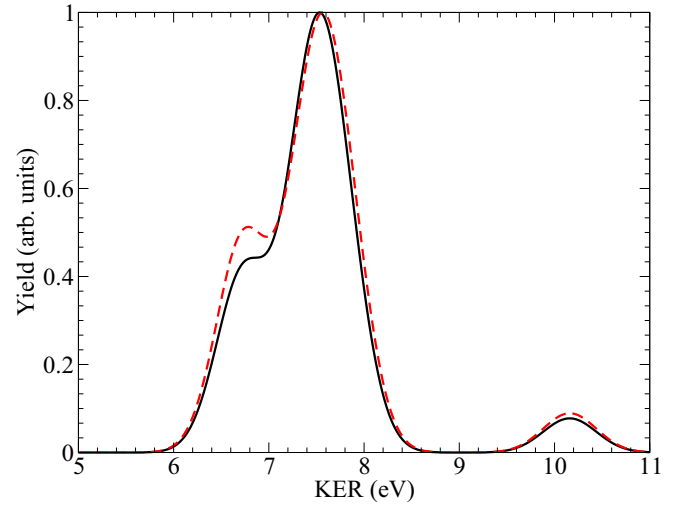


FIG. 7. Comparison of the normalized KER spectra with (solid) and without (dashed) the volume averaging. The peak laser intensity for both cases is $1.2 \times 10^{15}$ W/cm$^2$.

the $n$th state is [36]

$$\langle \overline{P_n}(I_0) \rangle = \int_0^{I_0} \overline{P_n}(I) \left( -\frac{\partial V}{\partial I} \right) dI,$$

$$-\frac{\partial V}{\partial I} = \frac{1}{I} \left( \frac{I_0}{I} + 2 \right) \sqrt{\frac{I_0}{I} - 1}, \tag{4}$$

where $I_0$ is the peak intensity. Note that the constants in the equation are omitted since the volume-averaged probabilities will be convoluted by Eq. (3) and the signal will then be normalized.

Figure 6 shows the intensity dependence of the integrand in Eq. (4) for states 5–9, with $I_0 = 1.2 \times 10^{15}$ W/cm$^2$. The yield is normalized to the peak yield of state 6. We see that the intensity that contributes the most is around 9–10 $\times$ 10$^{14}$ W/cm$^2$, which is not too far from the peak intensity. Therefore, the KER spectrum may not change much by the volume averaging. Indeed, the normalized KER spectra with and without volume averaging in Fig. 7 are almost identical, except volume averaging decreases the signal of the first peak, such that the ratio between the first to second peak of the volume-averaged spectrum is about 0.44.

### D. Alignment dependence

Alignment of N$_2$ molecules has been widely studied in many strong field experiments, yet as far as we know, there has been no study on the alignment dependence of dissociative SDI of N$_2$. Since the dissociative N$_2^{2+}$ states come from the removal of HOMO-1 ($1\pi_u$) or HOMO-2 ($2\sigma_u$), one expects that if the molecule is aligned or antialigned with the laser polarization, the yield for states 5–9 would change significantly. To simulate that effect, we introduce an alignment function $f$ in Eq. (2), such that

$$\bar{P}_n = \frac{1}{2} \int_0^\pi P_n(\theta) f(\theta) \sin \theta \, d\theta, \tag{5}$$

with $\int_0^\pi f(\theta) d\theta = 1$. The probabilities are then convoluted with Eq. (3) to obtain the KER signal. We consider four different alignments here: isotropic ($f = 1/\pi$), aligned ($f \propto \cos^6 \theta$), antialigned ($f \propto \cos^6(\theta - \pi/2)$), and 45° aligned [$f \propto \cos^6(\theta - \pi/4)$]. The laser parameters used here are the same as in Fig. 2.

Figure 8 shows the KER spectra with those four alignment functions. The spectra with aligned and antialigned N$_2$ show significant differences. Since ionization of a $\pi_u$ orbital (HOMO-1) is very weak when aligned, population of the $A$ state during ionization is strongly suppressed. Ionization from the $B$ state to state 6 is also suppressed since it involves ionizing the $\pi_u$ orbital. These lead to the overall suppression of the KER spectrum, with the peak at 7.6 eV being six times smaller than the isotropic case. On the contrary, in the case of antialignment, ionization of a $\pi_u$ orbital is preferred over $\sigma_{g/u}$ orbitals. Ionization to states 5, 7, and 8 are therefore enhanced
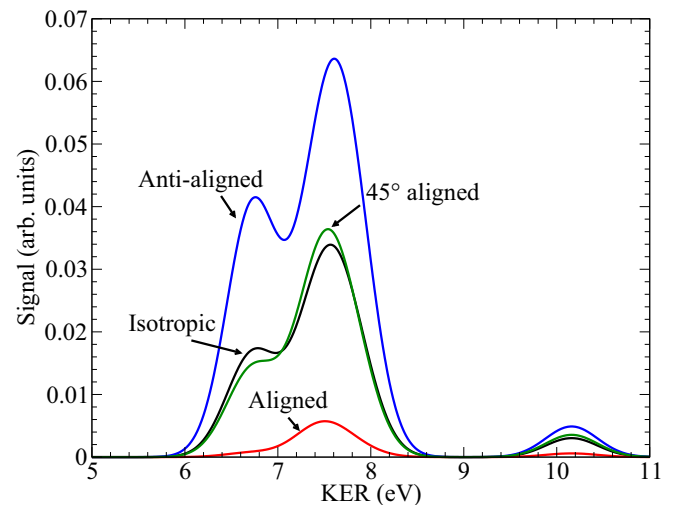


FIG. 8. KER spectra as in Fig. 2 with different alignment of the molecule.

since these states have two holes in the $\pi_u$ orbitals. In addition, during ionization, population of the $A$ state is enhanced while population of the $X$ and the $B$ states are suppressed. These lead to a fourfold and a twofold increase in the first and second peaks compared to the isotropic case. Interestingly, the spectrum for the 45° aligned case is very similar to the isotropic one since there is no strong preference in ionizing the $\pi_u$ or $\sigma_{g/u}$ orbitals.

Our results show that it is effective to control the KER spectrum of $N^+ + N^+$ by aligning the molecule, in consistence with the finding by Xie *et al.* [15] for $C_2H_2$. One can also deduce the symmetry of key intermediate states by changing the alignment. However, intermediate states with similar symmetry may not be distinguishable using this approach. In that case, one is then encouraged to control the KER spectrum and identify SDI pathways by changing the alignment as well as the wavelength of the laser.

## V. SUMMARY AND OUTLOOK

To summarize, we developed a simple and efficient model for SDI of molecules using a density-matrix approach. Our approach can describe the tunneling ionization of the neutral and ionic states and laser couplings between the same charged state at the same time. We applied the model to the SDI of $N_2$ with the use of the MO-ADK ionization rates for the first and second ionizations of the molecule. Angular-averaged yield for different $N_2^{2+}$ states were computed by solving the set of equations for density matrix of different charged states. By identifying dissociation limits and KER of different $N_2^{2+}$ states, the KER spectrum for $N^+ + N^+$ was calculated. We compared our simulated KER spectrum to the experiment by Voss *et al.* [21] and obtained a good agreement.

Taking advantage of the low computational cost, we explored different effects on the KER spectra. We first investigated the effect of laser couplings by neglecting the dipole moments in solving the ionic density matrix. We found that the angular-averaged yield of dissociative $N_2^{2+}$ states is at most a factor of 2 smaller without the laser coupling, such that laser couplings between the ionic states play an important role in the SDI of $N_2$. We then examined the effect of changing the laser wavelength to match the excitation energy from the $X$ to $A$ state and the $X$ to $B$ state of $N_2^+$. The KER spectrum from the 918- and 391-nm lasers does not show significant change compared to the spectrum from the 800-nm laser, but the latter spectrum does show some suppression on the first peak and enhancement on the second peak since the $B$ state is more populated during ionization. We also investigated the intensity dependence and focal volume effect on the angular-averaged yield of different $N_2^{2+}$ states. The onset of dissociative $N_2^{2+}$ states is at about $7 \times 10^{14}$ W/cm². The yield of most $N_2^{2+}$ states start to saturate from $1.2 \times 10^{15}$ W/cm²

and saturated at about $1.7 \times 10^{15}$ W/cm². The focal volume effect is therefore insignificant on the KER spectrum when the peak laser intensity is at about $1.2 \times 10^{15}$ W/cm². Finally, similar to the finding by Xie *et al.* [15], we found that the KER spectra change significantly in different alignment conditions. When the $N_2$ molecule is aligned or antialigned with laser polarization, the KER spectrum is strongly suppressed or enhanced. This further encourages the use of alignment to control the dissociation of doubly charged states of molecules. Since alignment of $N_2$ molecules has been well studied, we suggest that alignment dependence on dissociative SDI of $N_2$ to be investigated experimentally. Such experiments would provide additional data for unraveling the ionization dynamics and the structure of the target.

The good agreement between our results with the experiment by Voss *et al.* [21] shows the feasibility of using a simple model to simulate angle-integrated signal from the SDI of molecules. To further test the model, we plan to apply it to different molecular systems which have experimental data, such as $O_2$ [21], CO [37,38], NO [39], $CO_2$ [8], OCS [8], and $H_2O$ [8,10]. We could anticipate some challenges for the model when extending to other systems. For some ionic excited states, removing an electron from an orbital could lead to different doubly charged states with different ionization energies due to multielectron effects. For example, removing a spin-down electron from HOMO-1 ($1\pi_u$) of the $X^2\Pi_g$ state of $O_2^+$ could lead to the $^3\Delta_u$ or $^3\Sigma_u^-$ states of $O_2^{2+}$, which ionization energies are differed by about 1.2 eV at the equilibrium geometry of $O_2$ [40]. But, in a one-electron orbital model such as the MO-ADK theory, the binding energy of the $1\pi_{u+}$ and $1\pi_{u-}$ spin orbitals should be the same since they are degenerate, leading to ambiguity in the assignment of ionization energy. We will address this problem in our upcoming work.

Our present model can be extended to different pump-probe scenarios, provided that ionization rates at different nuclear geometries and at different electronic states are available. Therefore, our approach here could provide a theoretical foundation for interpreting molecular dynamics probed by intense short IR laser pulses. It could make pump-probe experiments of molecules more accessible and open up many more exciting research opportunities.

[1] J. Duris, S. Li, T. Driver, E. G. Champenois, J. P. MacArthur, A. A. Lutman, Z. Zhang, P. Rosenberger, J. W. Aldrich, R. Coffee *et al.*, Nat. Photonics **14**, 30 (2020).

[2] W. Decking, S. Abeghyan, P. Abramian, A. Abramsky, A. Aguirre, C. Albrecht, P. Alou, M. Altarelli, P. Altmann, K. Amyan *et al.*, Nat. Photonics **14**, 391 (2020).

[3] T. Gaumnitz, A. Jain, Y. Pertot, M. Huppert, I. Jordan, F. Ardana-Lamas, and H. J. Wörner, Opt. Express **25**, 27506 (2017).

[4] J. Li, J. Lu, A. Chew, S. Han, J. Li, Y. Wu, H. Wang, S. Ghimire, and Z. Chang, Nat. Commun. **11**, 2748 (2020).

[5] J. Ullrich, R. Moshammer, R. Dörner, O. Jagutzki, V. Mergel, H. Schmidt-Böcking, and L. Spielberger, J. Phys. B: At., Mol. Opt. Phys. **30**, 2917 (1997).

[6] J. Ullrich, R. Moshammer, A. Dorn, R. Dörner, L. P. H. Schmidt, and H. Schmidt-Böcking, Rep. Prog. Phys. **66**, 1463 (2003).

[7] A. T. Eppink and D. H. Parker, Rev. Sci. Instrum. **68**, 3477 (1997).

[8] S. Zhao, B. Jochim, P. Feizollah, J. Rajput, F. Ziaee, P. Kanaka Raju, B. Kaderiya, K. Borne, Y. Malakar, B. Berry, J. Harrington, D. Rolles, A. Rudenko, K. D. Carnes, E. Wells, I. Ben-Itzhak, and T. Severt, Phys. Rev. A **99**, 053412 (2019).

[9] N. Iwamoto, C. J. Schwartz, B. Jochim, K. Raju P., P. Feizollah, J. L. Napierala, T. Severt, S. N. Tegegn, A. Solomon, S. Zhao *et al.*, J. Chem. Phys. **152**, 054302 (2020).

[10] C. Cheng, Z. L. Streeter, A. J. Howard, M. Spanner, R. R. Lucchese, C. W. McCurdy, T. Weinacht, P. H. Bucksbaum, and R. Forbes, Phys. Rev. A **104**, 023108 (2021).

[11] T. Townsend, C. J. Schwartz, B. Jochim, K. Raju P., T. Severt, N. Iwamoto, J. L. Napierala, P. Feizollah, S. N. Tegegn, A. Solomon *et al.*, Front. Phys. **9**, 691727(2021).

[12] G. Basnayake, P. Hoerner, B. Mignolet, M. K. Lee, Y. F. Lin, A. H. Winney, D. A. Debrah, L. Popaj, X. Shi, X. K. Lee *et al.*, Phys. Chem. Chem. Phys. **23**, 23537 (2021).

[13] T. Severt, D. R. Daugaard, T. Townsend, F. Ziaee, K. Borne, S. Bhattacharyya, K. D. Carnes, D. Rolles, A. Rudenko, E. Wells *et al.*, Phys. Rev. A **105**, 053112 (2022).

[14] X.-M. Tong and C. D. Lin, Phys. Rev. A **70**, 023406 (2004).

[15] X. Xie, K. Doblhoff-Dier, H. Xu, S. Roither, M. S. Schöffler, D. Kartashov, S. Erattupuzha, T. Rathje, G. G. Paulus, K. Yamanouchi *et al.*, Phys. Rev. Lett. **112**, 163003 (2014).

[16] M. K. Lee, W. Li, and H. B. Schlegel, J. Chem. Phys. **152**, 064106 (2020).

[17] P. Hoerner, W. Li, and H. B. Schlegel, J. Chem. Phys. **155**, 114103 (2021).

[18] C. Guo, M. Li, and G. N. Gibson, Phys. Rev. Lett. **82**, 2492 (1999).

[19] Z. Wu, C. Wu, X. Liu, Y. Deng, Q. Gong, D. Song, and H. Su, J. Phys. Chem. A **114**, 6751 (2010).

[20] C. Beylerian and C. Cornaggia, J. Phys. B: At., Mol. Opt. Phys. **37**, L259 (2004).

[21] S. Voss, A. Alnaser, X.-M. Tong, C. M. Maharjan, P. Ranitovic, B. Ulrich, B. Shan, Z. Chang, C. D. Lin, and C. L. Cocke, J. Phys. B: At., Mol. Opt. Phys. **37**, 4239 (2004).

[22] A. S. Alnaser, S. Voss, X. M. Tong, C. M. Maharjan, P. Ranitovic, B. Ulrich, T. Osipov, B. Shan, Z. Chang, and C. L. Cocke, Phys. Rev. Lett. **93**, 113003 (2004).

[23] C. Wu, Y. Yang, Z. Wu, B. Chen, H. Dong, X. Liu, Y. Deng, H. Liu, Y. Liu, and Q. Gong, Phys. Chem. Chem. Phys. **13**, 18398 (2011).

[24] W. Eberhardt, E. W. Plummer, I. W. Lyo, R. Carr, and W. K. Ford, Phys. Rev. Lett. **58**, 207 (1987).

[25] H. Iwayama, T. Kaneyasu, Y. Hikosaka, and E. Shigemasa, J. Chem. Phys. **145**, 034305 (2016).

[26] M. Lundqvist, D. Edvardsson, P. Baltzer, and B. Wannberg, J. Phys. B: At., Mol. Opt. Phys. **29**, 1489 (1996).

[27] Q. Zhang, H. Xie, G. Li, X. Wang, H. Lei, J. Zhao, Z. Chen, J. Yao, Y. Cheng, and Z. Zhao, Commun. Phys. **3**, 50 (2020).

[28] D. Bhattacharya, K. Shamasundar, and A. Emmanouilidou, J. Phys. Chem. A **125**, 7778 (2021).

[29] S. R. Langhoff, C. W. Bauschlicher, Jr., and H. Partridge, J. Chem. Phys. **87**, 4716 (1987).

[30] S. R. Langhoff and C. W. Bauschlicher, Jr., J. Chem. Phys. **88**, 329 (1988).

[31] X.-M. Tong, Z. X. Zhao, and C. D. Lin, Phys. Rev. A **66**, 033402 (2002).

[32] S.-F. Zhao, C. Jin, A.-T. Le, T.-F. Jiang, and C. D. Lin, Phys. Rev. A **81**, 033423 (2010).

[33] S. Xue, S. Yue, H. Du, B. Hu, and A.-T. Le, Phys. Rev. A **104**, 013101 (2021).

[34] X.-M. Tong, Z. X. Zhao, A. S. Alnaser, S. Voss, C. L. Cocke, and C. D. Lin, J. Phys. B: At., Mol. Opt. Phys. **38**, 333 (2005).

[35] A. S. Alnaser, M. Zamkov, X. M. Tong, C. M. Maharjan, P. Ranitovic, C. L. Cocke, and I. V. Litvinyuk, Phys. Rev. A **72**, 041402(R) (2005).

[36] T. Morishita, Z. Chen, S. Watanabe, and C. D. Lin, Phys. Rev. A **75**, 023407 (2007).

[37] C. Cornaggia, J. Lavancier, D. Normand, J. Morellec, P. Agostini, J. P. Chambaret, and A. Antonetti, Phys. Rev. A **44**, 4499 (1991).

[38] J. Wu, L. P. H. Schmidt, M. Kunitski, M. Meckel, S. Voss, H. Sann, H. Kim, T. Jahnke, A. Czasch, and R. Dörner, Phys. Rev. Lett. **108**, 183001 (2012).

[39] C. Guo and G. N. Gibson, Phys. Rev. A **63**, 040701(R) (2001).

[40] M. Lundqvist, D. Edvardsson, P. Baltzer, M. Larsson, and B. Wannberg, J. Phys. B: At., Mol. Opt. Phys. **29**, 499 (1996).